RSC Advances

PAPER

View Article Online
View Journal | View Issue

Cite this: *RSC Adv.*, 2019, **9**, 42245

Biaxial strain modulated the electronic structure of hydrogenated 2D tetragonal silicene

Haoran Tu,[c] Jing Zhang,[a] Zexuan Guo[a] and Chunyan Xu *[ab]

Silicene-based materials have attracted great attention due to their easier incorporation into silicon-based devices and components. In addition to the reported hydrogenated 2D tetragonal silicene (γ-SiH), we propose two stable atomic configurations of hydrogenated 2D tetragonal silicene (α-SiH and β-SiH) based on first-principles calculation. The calculated results indicate hydrogenation can effectively open the band gap of 2D tetragonal silicene, α-SiH is a semiconductor with a direct band gap of 2.436 eV whereas β-SiH is indirect band gap of 2.286 eV. We also find that the electronic band structure of α-SiH, β-SiH and γ-SiH can be modulated *via* biaxial strain. By applying biaxial strain in the range of −10% to 12%, the band gap of α-SiH, β-SiH and γ-SiH can be tuned in a range of 1.732–2.585 eV. Furthermore, direct–indirect or indirect–direct transition can be induced under biaxial strain, showing a high degree of flexibility in electronic band structure. The research not only broadens the diversity of hydrogenated 2D tetragonal silicenes, but also provides more possibilities of their applications in spintronic devices.

Received 22nd October 2019
Accepted 16th December 2019

DOI: 10.1039/c9ra08634j

rsc.li/rsc-advances

1. Introduction

Silicene, as the cousin of graphene, has attracted great attention because of its easier incorporation into silicon-based devices and components. Silicene with a honeycomb structure is predicted to be stable and is studied theoretically.[1–4] Experimentally, silicene has been synthesized on different substrates.[5–8] Several two-dimensional (2D) allotropes of silicene have been proposed, such as MoS_2-type silicene,[9] tetra-silicene,[10] trigonal dumbbell silicene, honeycomb dumbbell silicene, large honeycomb dumbbell silicene,[11–13] and tetragonal silicone.[14,15] The physical properties in these materials mainly stem from the symmetry of the crystal structure. So, it is highly desirable to study 2D allotropes of materials with different symmetries. A 2D tetragonal allotrope in a square lattice consisting of tetrarings is also predicted to exist, including group IV[14–18] and V elements,[19,20] 2D BP[21] and SiC,[22] as well as transition-metal dichalcogenides.[23,24] The above studies reveal that some of the reported 2D tetragonal allotropes are nodal line semimetals or topological insulators. Subsequently, hydrogenated tetragonal Ge was reported to have two stable configurations, these configurations have a wide band gap which can be further tuned by external strain.[25] The recent study has found that 2D tetragonal silicene is stable and exhibits a nodal line semimetal nature.[14] Additionally, hydrogenation could induce a semimetal–semiconductor transition in 2D tetragonal silicene, this hydrogenated configuration (γ-SiH) is stable. Depending on the ordered distributions of H atoms, some possible configurations for hydrogenated 2D tetragonal silicene can be proposed, and the details of their structural and electronic properties have not been illustrated yet.

Hydrogenation can significantly change the properties of 2D materials and is reported to have potential applications in spintronic devices.[26–29] Theoretical predictions have revealed hydrogenation is an effective method to tailor the electronic properties of 2D silicene-related materials, and some of them have been observed in the experiments.[30–39] Recent studies have reported fully hydrogenated silicene becomes wide band gap semiconductor and the type of gap depending on its atomic conformation,[31] whereas half hydrogenated silicene transforms to ferromagnetic semiconductor.[32] In the experiments, half- and fully-hydrogenated silicene sheet have been studied and synthesized on Ag (1 1 1) substrate by using the scanning tunneling microscopy (STM), high-resolution electron energy loss spectroscopy (HREELS), angle-resolved photoelectron spectroscopy (ARPES) and low-energy electron diffraction (LEED).[35–39] The above works indicate atomic adsorption on nanosheet can be controlled with atomic precision in the experiments, which encourages use to modulate the properties of Si-based materials *via* adsorption. Moreover, the recently have reported the hydrogenated zigzag and armchair dumbbell silicene are semiconductors with larger band gaps, and their band gap and features are sensitive to strains.[30] To broaden the practical application of 2D silicon-based materials for spintronic devices, the band gap modulating is crucial. It is well known that strain engineering is a common way to tune the

[a]*Institute for Interdisciplinary Quantum Information Technology, Jilin Engineering Normal University, Changchun 130052, China. E-mail: xcy@jlenu.edu.cn*

[b]*Jilin Engineering Laboratory for Quantum Information Technology, Changchun 130052, China*

[c]*Key Laboratory of Physics and Technology for Advanced Batteries (Ministry of Education), Department of Physics, Jilin University, Changchun 130012, China*

band gap of 2D materials. Experimentally, methods for introducing strain into 2D materials generally include bending technique, piezoelectric stretching, exploiting the thermal expansion mismatch, elongating the substrate and controlled wrinkling, and so on.[40–46] For example, a direct–indirect transition is experimentally induced in monolayer WS_2 by applying uniaxial strain.[42] Monolayer 1T-HfS_2 is predicted theoretically to undergo a semiconductor–metal transition when compressive strain is applied.[47] The band gap of GaN monolayer can be modulated in the broad range of 4.44–2.27 eV by applying tensile strain.[48] In addition, monolayer GeP has been predicted to induce the transition from an indirect band-gap semiconductor to a direct band-gap semiconductor by the applied compressive strain along *a* direction.[49] It has been reported that external tensile strain can alter the band gap value of Ag_6S_2, and a direct–indirect transition occurs in Ag_6S_2 when the tensile strain exceeds a critical value.[50]

The above studies have revealed the properties of 2D materials can be tuned by surface modification and strain engineering. In this work, based on first-principles calculations, two stable atomic configurations of hydrogenated 2D tetragonal silicene (α-SiH and β-SiH) are proposed, and the stability, structural and electronic properties of them are illustrated. The effect of biaxial strain engineering on the structural and electronic properties of 2D hydrogenated tetragonal silicene (α-, β- and the reported γ-SiH) is also studied.

2. Computational details

All the calculations were based on the density functional theory (DFT) as implemented in the Vienna *Ab initio* Simulation Package (VASP).[51–53] The electron–ion interactions were described by projector-augmented wave (PAW) method,[54] and exchange–correlation functional was considered in the generalized gradient approximation (GGA)[55] with Perdew–Burke–Ernzerhof (PBE) functional. The plane wave basis was set to be 500 eV and the Brillouin zone (BZ) was sampled of a $13 \times 13 \times 1$ *k*-point mesh. All structures were fully relaxed until the force exerted on each atom was less than 0.01 eV $Å^{-1}$ and the total energy change was smaller than 1×10^{-6} eV. A vacuum layer more than 20 Å was placed to minimize the interaction between periodic images along the *z*-direction. In addition, the hybrid Heyd–Scuseria–Ernzerhof (HSE06) functional[56] was used to check the validity of the band gap given by the PBE method. The *ab initio* molecular dynamics (AIMD) simulations were implemented based on the NVT ensemble with a time step of 1 fs and the total simulation time of 10 ps. The phonon dispersions were performed by using the PHONOPY code.[57]

3. Results and discussion

Fig. 1 presents the optimized atomic configurations of hydrogenated 2D tetragonal silicene denoted by α-SiH, β-SiH and γ-SiH, respectively. The γ-SiH has been studied previously[14] while α-SiH and β-SiH have not been investigated yet. In the case of α-SiH and β-SiH, the hydrogen atoms alternate in pairs of the sheet in different ways. For γ-SiH, the hydrogen atoms alternate on both sides of the sheet. All studied structures have a square lattice, each Si atom bonded with other three Si atoms and one H atom. The optimized structural parameters of these three configurations are summarized in Table 1. All the Si–Si bond lengths in three hydrogenated systems are larger than those in the pure tetragonal silicene. The buckled height h_0 of α-SiH is much larger than those of β-SiH and γ-SiH, and they are larger than the buckled height h_0 of pure tetragonal silicene. The hydrogenated 2D tetragonal silicene (γ-SiH) is stable that has been reported previously.[14] So next we just discuss the stability of α-SiH and β-SiH by calculating the binding energy, phonon dispersions and AIMD simulations. The binding energy for hydrogenated 2D tetragonal silicene defined by $E_b = (E_{SiH} - nE_{Si} - nE_H)/2n$, where E_{SiH} is the total energy of hydrogenated 2D tetragonal silicene, E_{Si} and E_H are the energy of the single Si and single H atom, respectively. And *n* is the number of Si or H atom in the unit cell.

The binding energy E_b is firstly calculated and listed in Table 1. The resulting binding energies of α-SiH (−3.339 eV per atom) and β-SiH (−3.259 eV per atom) are closed to that of fully hydrogenated silicene (−3.373 eV per atom).[31] This illustrates that hydrogenation is an energetically favorable process on the 2D tetragonal silicene in terms of these two configurations. Then, AIMD simulations are performed for α-SiH and β-SiH monolayer

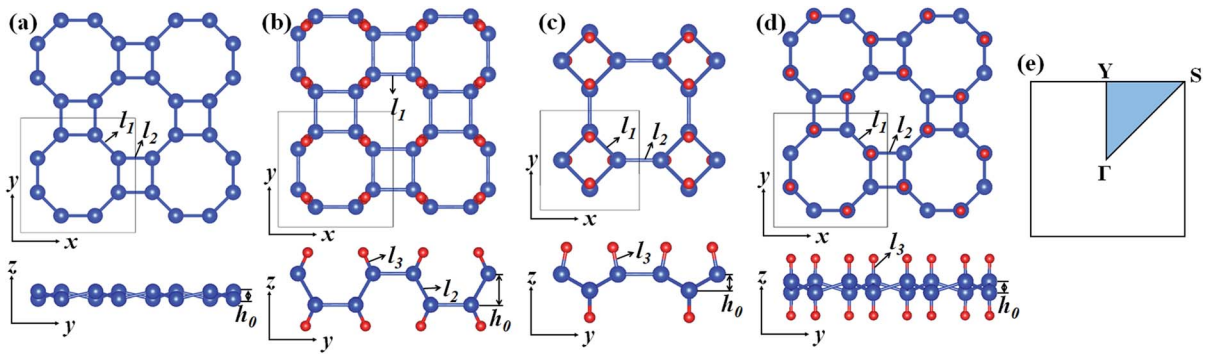

Fig. 1 Geometric structures of (a) pure tetragonal silicene, (b) α-SiH, (c) β-SiH and (d) γ-SiH. The unit cell is marked with a solid box, the blue and red balls stand for Si and H atoms, respectively. (e) First Brillouin zone with high-symmetry points labeled.

Table 1 The structural parameters, binding energy and band gap of pure tetragonal silicene, α-SiH, β-SiH and γ-SiH: lattice constant a_0; bond lengths l_1, l_2 and l_3; buckled height h_0; binding energy E_b; band gap E_g

System	a_0 (Å)	l_1 (Å)	l_2 (Å)	l_3 (Å)	h_0 (Å)	E_b (eV per atom)	E_g (eV)
Si	7.611	2.307	2.249	—	0.491	—	—
α-SiH	6.813	2.380	2.345	1.501	1.840	−3.339	2.436
β-SiH	5.458	2.367	2.357	1.502	0.889	−3.259	2.414
γ-SiH	7.660	2.370	2.339	1.500	0.723	−3.340	2.286

at 300 K of 10 ps to check their thermal stability. The fluctuations of total energies with simulation time and the final structures are plotted in Fig. 2a. It can be seen that the total energies show slightly fluctuation during the entire simulation and there are no structural reconstruction for both α-SiH and β-SiH, which confirms their structures are thermally stable at room temperature. To further test the dynamical stability of α-SiH and β-SiH, the phonon dispersions are calculated and displayed in Fig. 2b and c. In the case of α-SiH, there is a very small imaginary frequency about -0.97 cm^{-1} near the Γ point, this small instability may be caused by the artifacts of numeric when using first-principles calculations for 2D layers. The larger imaginary frequencies have been reported in 1T′-MX_2 (M = Mo, W; X = S, Se, Te),[58] these systems have been synthesized in the experiments.[59–63] Thus, α-SiH is dynamically stable. As shown in Fig. 2c, there is no imaginary frequency in the whole BZ for β-SiH, confirming the dynamical stability of β-SiH.

To study the effect of hydrogenation on the electronic structure of 2D tetragonal silicene, the electronic properties of α-, β- and γ-SiH with equilibrium lattice constant have been studied and band structures are displayed in Fig. 3. The results show that these three configurations are semiconductor with a direct band gap of 2.436 eV and 2.286 eV for α-SiH and γ-SiH, and indirect band gap of 2.414 eV for β-SiH. Thus, hydrogenation can effectively open the band gap of 2D tetragonal silicene and change it from a semimetal to a semiconductor. As shown in Fig. 3, the valence band maxima (VBM) of α-, β- and γ-SiH lies at Γ point, and the conduction band minima (CBM) of both α-SiH and γ-SiH lies at Γ point while the CBM occurs along the Γ–Y direction for β-SiH. By projecting the bands onto different atomic orbitals, it can be seen from Fig. 3 that the VBM is mostly consist of Si-p_{xy} orbitals for three configurations, while the CBM is dominated by Si-p_z orbitals for α-SiH and Si-s orbitals for both

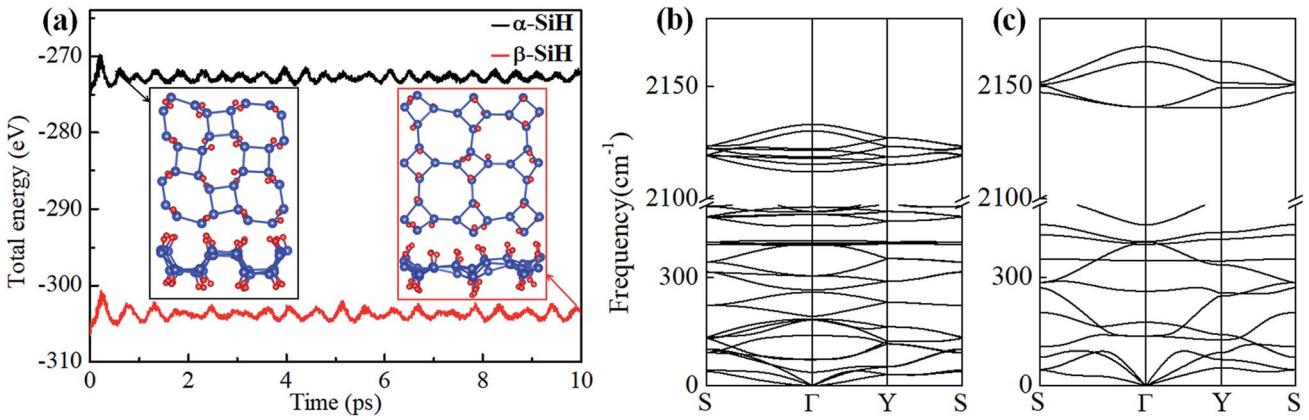

Fig. 2 (a) Total energy fluctuations of α-SiH (black line) and β-SiH (red line) with respect to time in AIMD simulations at 300 K, the insets show the final structures at the end of 10 ps. Phonon dispersion of (b) α-SiH and (c) β-SiH.

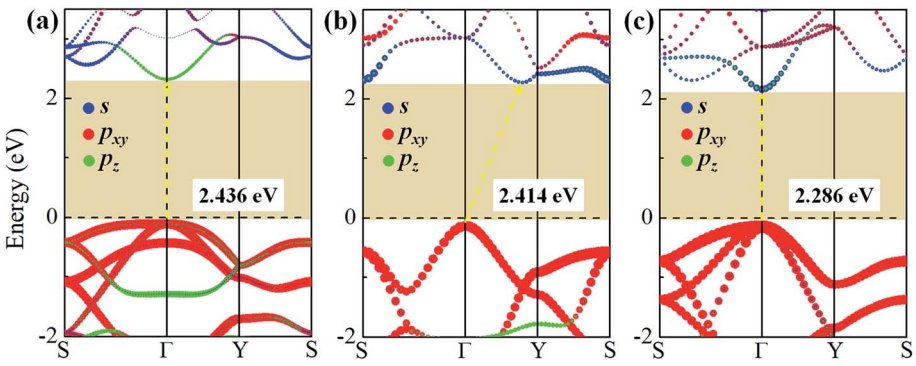

Fig. 3 The projection electronic band structures of (a) α-SiH, (b) β-SiH and (c) γ-SiH, where the blue, red and green dots describe the contribution from s, p_{xy}, and p_z orbitals of Si atoms, respectively. The Fermi level is set to zero and denoted by a dashed line.

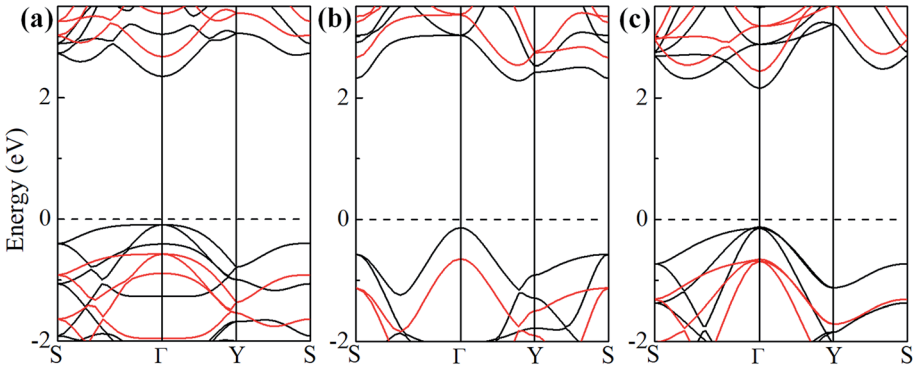

Fig. 4 Band structures of (a) α-SiH, (b) β-SiH and (c) γ-SiH. The black and red lines in the band structures represent PBE and HSE06 calculations, respectively. The Fermi level is set to zero and denoted by a dashed line.

of β- and γ-SiH. The calculated band structure of γ-SiH is consistent with previous results reported by Wu *et al.*[14] To verify the validity of the band gaps by PBE calculation, the HSE06 calculation is used to check the electronic band structure of those three systems. As shown in Fig. 4, the band gaps of α-SiH, β-SiH and γ-SiH at HSE06 calculation are increased to 3.244 eV, 3.177 eV and 3.090 eV, respectively, while the overall electronic band profiles calculated by PBE and HSE06 calculations are similar for three systems. The present work is mainly focused on the biaxial strain effect on the band structure of these three systems, although the band gaps are underestimated by PBE calculation, it is still be able to predict the general trends of strain effect on the band structures in α-SiH, β-SiH and γ-SiH.

It is well known that tailoring electronic properties of semiconductor materials is very critical for potential applications, strain engineering is one of the effective approaches to regulate the electronic properties of semiconductors. Here, we investigated the structural and electronic properties of α-, β- and γ-SiH under an external biaxial strain within the range of −10% to 12%. The biaxial strain is described as $\varepsilon = (a - a_0)/a_0 \times 100\%$, where a_0 and a are the lattice constants of unstrained and strained systems, respectively. For the strained system, just atomic position is allowed to relax. Hereinto, strains in the range of −10% to 12% with spacing of 2% are considered, negative and positive values of strain ε refer to compressive and tensile strains, respectively. Fig. 5a gives the system energy, the variational ratio of bond lengths (l_1, l_2 and l_3) and buckled height h_0 as a function of biaxial strain. As seen in Fig. 5a, the energies increase with biaxial strain increases in a quadratic way for these three atomic configurations. The energy of β-SiH is larger than that of α-SiH and γ-SiH under different biaxial strains from −10% to 12%. The γ-SiH is energetically more stable than α-SiH with biaxial strain in the range of $-2\% \leq \varepsilon \leq 2\%$, while α-SiH is more stable than γ-SiH when biaxial strains exceed ±2%. The variational ratio of bond lengths and buckled height with respect to biaxial strain is displayed in Fig. 5b. The variational ratio of bond lengths and buckled height are defined as $\Delta l = (L_i - l_i)/l_i$ and $\Delta h = (h - h_0)/h_0$, respectively, where L_i (i = 1, 2 and 3) and h signify the bond lengths and buckled height in strained system. For α-SiH system, it can be found that the variations of bond lengths l_1 and l_2 increase monotonously while bond length l_3 is almost unchanged, and the

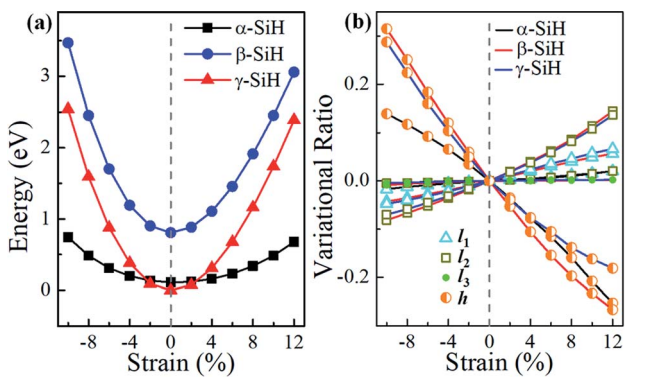

Fig. 5 (a) System energy, (b) bond lengths and buckled height for α-SiH, β-SiH and γ-SiH as a function of biaxial strain.

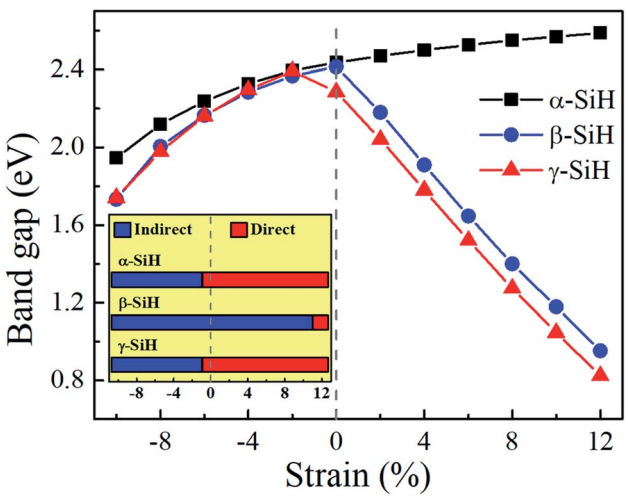

Fig. 6 The Variation of band gap with respect to biaxial strain for α-SiH, β-SiH and γ-SiH. The insets show the schematic drawings of the gap type transition for three atomic configurations under the corresponding biaxial strain. The blue and red rectangles represent indirect and direct band gaps, respectively.

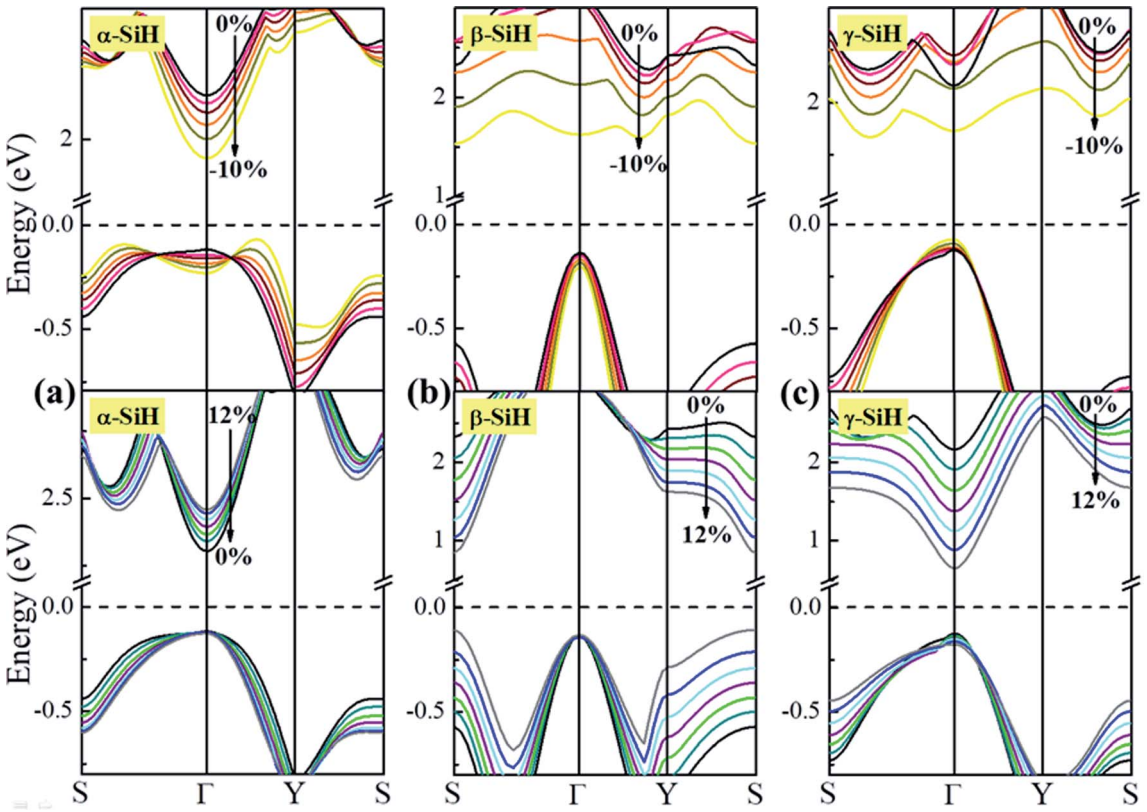

Fig. 7 The band structures under different biaxial strain for (a) α-SiH, (b) β-SiH and (c) γ-SiH. The Fermi level is set to zero and denoted by a dashed line.

buckled height h_0 decreases monotonously for α-SiH under biaxial strain from −10% to 12%. The similar process can be found in the strained β-SiH and γ-SiH, just the variations in bond lengths l_1 and l_2 (buckled height h_0) increase (decrease) more quickly.

Now, we discuss the modulations of electronic band structures in α-, β- and γ-SiH by applying biaxial strain from −10% to 12%. The band gaps and band structures of three configurations under different strain are shown in Fig. 6 and 7, respectively. In Fig. 6, the band gap of α-SiH increases linearly within the tensile strain range from 0% to 12%, and it reduces under enhanced compressive strains in the range of 0% to −10%. As shown in Fig. 7a, there is a direct-to-indirect transition in α-SiH due to compressive strain, it shows an indirect band gap when the system is strained at −2%, where the location of the VBM lies along the S–Γ direction whereas the CMB remains at the Γ point. In the case of β-SiH, the band gap is reduced by applying either tensile or compressive strain as plotted in Fig. 6. It can be seen from Fig. 7b, the β-SiH can be transformed from an indirect character to direct character with both of the VBM and CBM lie at the S point, and the critical strain for indirect–direct transition is 12%. As seen in Fig. 6, the band gap of γ-SiH decreases with tensile strain increases whereas the band gap increases and then it decreases as the compressive strain increases, and the band gap of γ-SiH reaches a maximal value at −2% strain. When the compressive strain increases to −2%, the γ-SiH undergoes a transition from direct band gap to indirect band gap with its VMB still locating at Γ-point and CBM shifting from Γ point to a midpoint along S–Γ direction, as depicted in Fig. 7c.

4. Conclusions

In conclusion, in addition to the reported hydrogenated 2D tetragonal silicene (γ-SiH), the other two atomic configurations of hydrogenated 2D tetragonal silicene (α-SiH and β-SiH) have been proposed. The calculated binding energy, AIMD simulations and phonon dispersions indicate that both of α-SiH and β-SiH are stable. Both of them are semiconductors, the α-SiH has a direct band gap of 2.436 eV and β-SiH displays an indirect band gap of 2.286 eV. When applying external strain from −10% to 12%, the β-SiH is less stable than α-SiH and γ-SiH, γ-SiH is energetically more stable than α-SiH in the strain range of $-2\% \leq \varepsilon \leq 2\%$ while α-SiH is more stable than γ-SiH when biaxial strains exceed ±2%. Furthermore, the electronic band structures and band gap type of α-SiH, β-SiH and γ-SiH can be effectively regulated by applying external biaxial strain. By means of biaxial strain, these three configurations experience direct–indirect or indirect–direct transition, and the band gap can be tuned in a range of 1.732–2.585 eV.

Conflicts of interest

There are no conflicts to declare.

Acknowledgements

This work was supported by the Specialized Fund for the Doctoral Research of Jilin Engineering Normal University under Grants No. BSKJ201904.

References

1 Z. Ni, Q. Liu, K. Tang, J. Zheng, J. Zhou, R. Qin, Z. Gao, D. Yu and J. Lu, *Nano Lett.*, 2012, **12**, 113–118.
2 H. Liu, J. Gao and J. Zhao, *J. Phys. Chem. C*, 2013, **117**, 10353–10359.
3 C.-C. Liu, W. Feng and Y. Yao, *Phys. Rev. Lett.*, 2011, **107**, 076802.
4 X. Li, J. T. Mullen, Z. Jin, K. M. Borysenko, M. Buongiorno Nardelli and K. W. Kim, *Phys. Rev. B: Condens. Matter Mater. Phys.*, 2013, **87**, 115418.
5 B. Feng, Z. Ding, S. Meng, Y. Yao, X. He, P. Cheng, L. Chen and K. Wu, *Nano Lett.*, 2012, **12**, 3507–3511.
6 A. Fleurence, R. Friedlein, T. Ozaki, H. Kawai, Y. Wang and Y. Yamada-Takamura, *Phys. Rev. Lett.*, 2012, **108**, 245501.
7 C. Grazianetti, E. Cinquanta and A. Molle, *2D Mater.*, 2016, **3**, 012001.
8 L. Meng, *et al.*, *Nano Lett.*, 2013, **13**, 685–690.
9 F. Gimbert, C.-C. Lee, R. Friedlein, A. Fleurence, Y. Yamada-Takamura and T. Ozaki, *Phys. Rev. B: Condens. Matter Mater. Phys.*, 2014, **90**, 165423.
10 M. Qiao, Y. Wang, Y. Li and Z. Chen, *J. Phys. Chem. C*, 2017, **121**, 9627–9633.
11 S. Cahangirov, V. O. Özçelik, A. Rubio and S. Ciraci, *Phys. Rev. B: Condens. Matter Mater. Phys.*, 2014, **90**, 085426.
12 S. Cahangirov, V. O. Özçelik, L. Xian, J. Avila, S. Cho, M. C. Asensio, S. Ciraci and A. Rubio, *Phys. Rev. B: Condens. Matter Mater. Phys.*, 2014, **90**, 035448.
13 F. Matusalem, M. Marques, L. K. Teles and F. Bechstedt, *Phys. Rev. B: Condens. Matter Mater. Phys.*, 2015, **92**, 045436.
14 H. Wu, Y. Qian, Z. Du, R. Zhu, E. Kan and K. Deng, *Phys. Lett. A*, 2017, **381**, 3754–3759.
15 Z. Zhuo, X. Wu and J. Yang, *Nanoscale*, 2018, **10**, 1265–1271.
16 N. Jawad, J. Xue, P. Biswarup, Z. Jijun, K. Tae Won and A. Rajeev, *Nanotechnol*, 2012, **23**, 385704.
17 Y. Liu, G. Wang, Q. Huang, L. Guo and X. Chen, *Phys. Rev. Lett.*, 2012, **108**, 225505.
18 C. Xu, Y. Wang, R. Han, H. Tu and Y. Yan, *New J. Phys.*, 2019, **21**, 033005.
19 K. Liangzhi, T. Xin, M. Yandong, T. Hassan, Z. Liujiang, S. Ziqi, A. Du, C. Changfeng and C. S. Sean, *2D Mater.*, 2015, **2**, 045010.
20 Y. Zhang, J. Lee, W.-L. Wang and D.-X. Yao, *Comput. Mater. Sci.*, 2015, **110**, 109–114.
21 Z. Zhu, X. Cai, C. Niu, C. Wang and Y. Jia, *Appl. Phys. Lett.*, 2016, **109**, 153107.
22 C. Yang, Y. Xie, L.-M. Liu and Y. Chen, *Phys. Chem. Chem. Phys.*, 2015, **17**, 11211–11216.
23 S. M. Nie, Z. Song, H. Weng and Z. Fang, *Phys. Rev. B: Condens. Matter Mater. Phys.*, 2015, **91**, 235434.
24 A. M. van der Zande, P. Y. Huang, D. A. Chenet, T. C. Berkelbach, Y. You, G.-H. Lee, T. F. Heinz, D. R. Reichman, D. A. Muller and J. C. Hone, *Nat. Mater.*, 2013, **12**, 554.
25 C. Xu, J. Zhang, M. Guo and L. Wang, *RSC Adv.*, 2019, **9**, 23142–23147.
26 J. Li, H. Li, Z. Wang and G. Zou, *Appl. Phys. Lett.*, 2013, **102**, 073114.
27 A. Lopez-Bezanilla, P. Ganesh, P. R. C. Kent and B. G. Sumpter, *Nano Res.*, 2014, **7**, 63–70.
28 W. X. Zhang, H. Wang, C. H. Shi, S. Y. Liu, S. Y. Chang and C. He, *J. Phys. Chem. C*, 2019, **123**, 14999–15008.
29 J. Zhou, Q. Wang, Q. Sun and P. Jena, *Phys. Rev. B: Condens. Matter Mater. Phys.*, 2010, **81**, 085442.
30 Y. Ding and Y. Wang, *J. Phys. Chem. C*, 2018, **122**, 23208–23216.
31 Y. Ding and Y. Wang, *Appl. Phys. Lett.*, 2012, **100**, 083102.
32 X.-Q. Wang, H.-D. Li and J.-T. Wang, *Phys. Chem. Chem. Phys.*, 2012, **14**, 3031–3036.
33 Y. Ding and Y. Wang, *J. Mater. Chem. C*, 2015, **3**, 11341–11348.
34 M. Houssa, E. Scalise, K. Sankaran, G. Pourtois, V. V. Afanas'ev and A. Stesmans, *Appl. Phys. Lett.*, 2011, **98**, 223107.
35 J. Qiu, H. Fu, Y. Xu, A. I. Oreshkin, T. Shao, H. Li, S. Meng, L. Chen and K. Wu, *Phys. Rev. Lett.*, 2015, **114**, 126101.
36 J. Qiu, H. Fu, Y. Xu, Q. Zhou, S. Meng, H. Li, L. Chen and K. Wu, *ACS Nano*, 2015, **9**, 11192–11199.
37 W. Wang, W. Olovsson and R. I. G. Uhrberg, *Phys. Rev. B*, 2016, **93**, 081406.
38 D. Solonenko, V. Dzhagan, S. Cahangirov, C. Bacaksiz, H. Sahin, D. R. T. Zahn and P. Vogt, *Phys. Rev. B*, 2017, **96**, 235423.
39 D. B. Medina, E. Salomon, G. Le Lay and T. Angot, *J. Electron Spectrosc. Relat. Phenom.*, 2017, **219**, 57–62.
40 Y. Y. Hui, X. Liu, W. Jie, N. Y. Chan, J. Hao, Y.-T. Hsu, L.-J. Li, W. Guo and S. P. Lau, *ACS Nano*, 2013, **7**, 7126–7131.
41 G. Plechinger, A. Castellanos-Gomez, M. Buscema, H. S. J. van der Zant, G. A. Steele, A. Kuc, T. Heine, C. Schüller and T. Korn, *2D Mater.*, 2015, **2**, 015006.
42 Y. Wang, C. Cong, W. Yang, J. Shang, N. Peimyoo, Y. Chen, J. Kang, J. Wang, W. Huang and T. Yu, *Nano Res.*, 2015, **8**, 2562–2572.
43 S. Yang, *et al.*, *Nano Lett.*, 2015, **15**, 1660–1666.
44 A. Castellanos-Gomez, R. Roldán, E. Cappelluti, M. Buscema, F. Guinea, H. S. J. van der Zant and G. A. Steele, *Nano Lett.*, 2013, **13**, 5361–5366.
45 Y. Wang, C. Cong, R. Fei, W. Yang, Y. Chen, B. Cao, L. Yang and T. Yu, *Nano Res.*, 2015, **8**, 3944–3953.
46 Y. Li, Z. Hu, S. Lin, S. K. Lai, W. Ji and S. P. Lau, *Adv. Funct. Mater.*, 2017, **27**, 1600986.
47 N. Wu, X. Zhao, X. Ma, Q. Xin, X. Liu, T. Wang and S. Wei, *Phys. E*, 2017, **93**, 1–5.
48 H. Shu, X. Niu, X. Ding and Y. Wang, *Appl. Surf. Sci.*, 2019, **479**, 475–481.
49 Q.-Y. Chen, C. Cao and Y. He, *Phys. E*, 2019, **113**, 172–180.
50 F. Ersan, *Comput. Mater. Sci.*, 2019, **163**, 278–281.

51 G. Kresse and J. Furthmüller, *Phys. Rev. B: Condens. Matter Mater. Phys.*, 1996, **54**, 11169–11186.
52 G. Kresse and J. Hafner, *Phys. Rev. B: Condens. Matter Mater. Phys.*, 1993, **47**, 558–561.
53 G. Kresse and J. Hafner, *Phys. Rev. B: Condens. Matter Mater. Phys.*, 1994, **49**, 14251–14269.
54 P. E. Blöchl, *Phys. Rev. B: Condens. Matter Mater. Phys.*, 1994, **50**, 17953–17979.
55 J. P. Perdew, K. Burke and M. Ernzerhof, *Phys. Rev. Lett.*, 1996, **77**, 3865–3868.
56 J. Heyd, G. E. Scuseria and M. Ernzerhof, *J. Chem. Phys.*, 2003, **118**, 8207–8215.
57 D. Alfè, *Comput. Phys. Commun.*, 2009, **180**, 2622–2633.
58 D. B. Putungan, S.-H. Lin and J.-L. Kuo, *Phys. Chem. Chem. Phys.*, 2015, **17**, 21702–21708.
59 S.-Y. Chen, C. H. Naylor, T. Goldstein, A. T. C. Johnson and J. Yan, *ACS Nano*, 2017, **11**, 814–820.
60 G. H. Han, *et al.*, *2D Mater.*, 2016, **3**, 031010.
61 J. Lee, F. Ye, Z. Wang, R. Yang, J. Hu, Z. Mao, J. Wei and P. X. L. Feng, *Nanoscale*, 2016, **8**, 7854–7860.
62 A. P. Nayak, *et al.*, *Nano Lett.*, 2015, **15**, 346–353.
63 Q. Song, H. Wang, X. Pan, X. Xu, Y. Wang, Y. Li, F. Song, X. Wan, Y. Ye and L. Dai, *Sci. Rep.*, 2017, **7**, 1758.